Article:
Wu, L., Palamarciuc, I., Bajwa, R. et al. (2 more authors) (2026) An in-situ wear measurement instrumentation for thin metallic bearing coatings using high frequency ultrasound. Tribology International. 111267. ISSN: 0301-679X

https://doi.org/10.1016/j.triboint.2025.111267

An In-Situ Wear Measurement Approach for Thin Metallic Bearing Coatings Using High Frequency Ultrasound

Liqun Wu [a], Ion Palamarciuc [b], Rizwan Bajwa [b], Yi Zhang [b], R S Dwyer-Joyce [a, *]

a. Department of Mechanical Engineering, The University of Sheffield, Sheffield, UK

b. R&D Department, Daido Metal Co., Ltd European Technical Centre (UK), Somerset, UK

Abstract: Plain bearings are widely used in a variety of applications and industries, due to their relative low cost, simplicity, and reliability. The bearing usually consists of a steel shell with a softer metal or polymeric surface layer. The softer surface layer is designed to facilitate running in and act as a low friction sacrificial layer in case of lubricant starvation. Their maintenance and diagnosis are usually achieved by visual inspection after disassembly which leads to downtime losses. In this paper, an in-situ monitoring technique for bearing wear status has been achieved through a bespoke ultrasound-based sensing system. High frequency 22MHz multiplexed ultrasound signals were used to inspect the thin bearing coating at different locations and in a real time. Numerical wave propagation simulations were performed to show the signal sensitivity to various wear cases. In-situ experiments have shown that the system can measure the real-time thickness of the surface coating during the machine operation with a high accuracy. The research underpins the design of a prototype for an in-situ plain bearing wear sensor instrument.

Key words: Ultrasound Measurement, In-situ Wear Measurement, Plain Bearings

1. Introduction

The advantages of plain journal bearings lie in their low cost and ease of replacement. They are designed to wear out preferentially to protect an expensive shaft. The bearing shell, a common plain bearing component, is generally made of a steel backing with a soft metal or polymer wear-resistant liner to extend its service life. Because bearing shells use oil film lubrication unlike precision rollers, they can absorb greater external impact, making them more stable and reliable under these working situations with potential shocks and vibrations [1].

In terms of service life, in principle, the life of a bearing shell working in the fully lubricated hydrodynamic regime should be infinite. However, due to overload, oil starvation, contamination, or other reasons, the bearings might be unintentionally used under a mixed or boundary lubricated condition, which means structural damage can occur on the inner surface of the bearing [2], [3]. This means that the bearing shells need to be maintained and, in some applications, replaced regularly. Therefore, if the structural health of a bearing can be monitored in real time during operation, the unnecessary maintenance costs and downtime losses can be effectively reduced. Compared with other non-destructive testing methods, the advantage of ultrasound lies in its small sensor size and low hazard to human. In a compact rotary system, a millimeter sized ultrasound sensor is possible for condition monitoring.

Detection of thin layers of an acoustically dissimilar material on a free surface with ultrasound can be challenging. Palmer et al. measured 11μm of epoxy resin coating on a 220μm thick

aluminium plate using a resonance method with radially polarized shear sensors [4]. Kanja et al. proposed using ultrasound to excite standing waves in materials and receiving them using another ultrasound sensor (Pitch-Catch), which proved that this method could detect four discrete epoxy resin thicknesses between 70-140µm, and it was estimated that the minimum detection thickness was about 39µm when the sensor center frequency was 19.5MHz [5]. Regarding long-term and continuous in-situ monitoring, in 1997, Long et al. used pulse echo technology for the detection of wear in titanium alloys [6]. Brunskill et al. employed a 10MHz ultrasound sensor to monitor the wear of an aluminium workpiece in real-time during wear experiments by using ultrasound reflection. The aluminium workpiece was subjected to friction by a rotating disk [7]. Similarly, in 2013, Honarvar et al. devised a long-term corrosion measurement system for industrial pipelines, which involved attaching an ultrasound sensor with a delay line to the outer wall of the pipeline and monitoring the thickness of the pipe wall through echo. However, it should be noted that the coating measurement discussed above are almost working in an off-line condition. And for a continuous monitoring, the objective is a single-layer plate and there is little research on complex multi-layer or thin-layer structures [8].

In this paper, a pulse-echo based on-line measurement system is proposed, with 22MHz high-frequency ultrasound sensors and with high-frequency multiplexer (MUX). A data acquisition system based on a digital oscilloscope and micro-controller Arduino has been designed to drive the sensors and MUX. Based on a series of in-situ experiments, wear progression has been monitored using the ultrasonic signal and associated temperature data.

2. In-Situ Ultrasound System Design

2.1 Ultrasound Sensors

To measure the bearing components with a high-frequency sensor, a shell mounted ultrasound sensor design has been proposed, where the sensor is tightly connected to the surface of bearing shell through conductive epoxy. A lead zirconate titanate (PZT) piezo-element DL50-HD from DEL Piezo Ltd has been selected as the material of ultrasound sensors. The design diagram is shown in Figure 1-a. The size of sensor is approximately 2mmx1mm to accommodate the curvature of the outer surface of the bearing shell. The sensor is supplied pre-coated on both sides with a silver coating to act as the electrode. The sensor bottom surface shares the ground with the bearing shell and the test signal is applied to the top surface. Ultrasound sensors are installed in locations where bearings are prone to damage, usually in areas with high stress distribution, for example, the loaded area at top center. A coaxial cable with jump wires is used for the signal transmission and a mixture of epoxy and tungsten powder is used for solder joint protection and damping sensor ringing. Figure 1-b shows an example of the instrumented bearing.

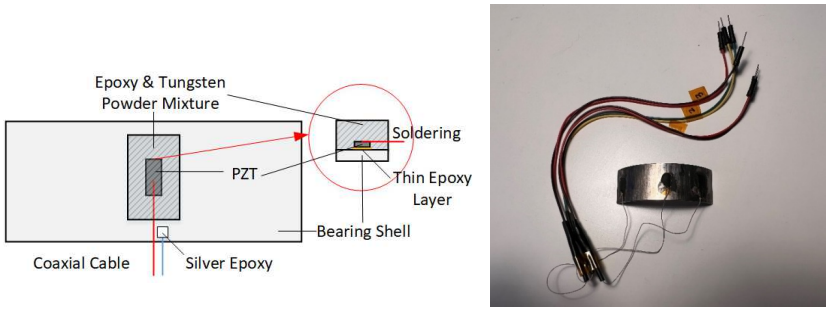

(a) (b)

Figure 1. (a) Design of the bearing shell-mounted sensor (b) Bearing shell with installed sensors

2.2 Ultrasound Data Acquisition Module

Figure 2 shows the instrumentation design of the ultrasound testing system. The entire system is based on pulse-echo technique and the data from sensors is collected by a digital oscilloscope, which is then transmitted back to a computer and recorded for processing. The hardware consists of a digital oscilloscope PicoScope used for transmitting and receiving electrical signals, and a digital acquisition (DAQ) card TC-08 used for temperature recording. A micro-controller Arduino Uno is used to control the multiplexer TMUX1109 to achieve multi-channel acquisition of ultrasound signals. The software used was a virtual instrument based on LabVIEW to control the above components.

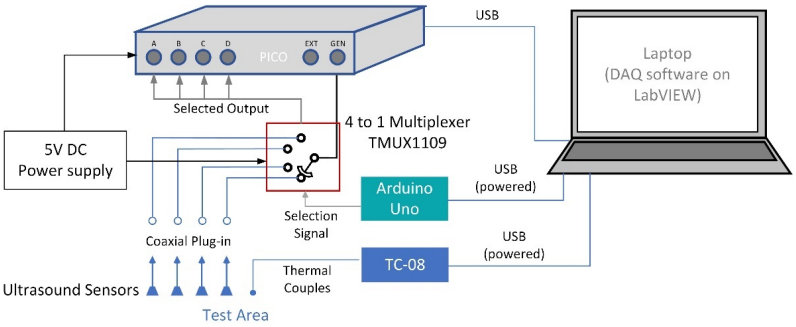

Figure 2. The in-Situ ultrasound bearing shell measurement instrumentation

In the DAQ module the data collection is divided into two parts. The first is ultrasound signal collection based on the digital oscilloscope PicoScope 5444D, which is used for sending and receiving electric signals. The second is a temperature DAQ TC08, which can be connected with eight thermocouples. In the system, K-type thermocouples have been used, which are a base metal thermocouple made from conductors containing Nickel-Chromium and Nickel-Aluminium alloys. For K-type thermocouples, the detection range of TC08 is -270°C to 1370°C.

According to Nyquist's Law of Sampling, the sampling frequency of analog signal should be at least twice the center frequency of signal. For a 22MHz sensor, the frequency for ultrasound DAQ system should be at least 44MHz. Therefore, for DAQ settings, 8-bit mode was used, and the single channel sampling rate was set to 500MS/s, which means that the time interval between each sampling point is 2ns. The key parameters of PicoScope 5444D are given in Table 1.

Table 1. Key parameters for the analog data acquisition of PicoScope 5444D

Bandwidth (-3dB)	***Input Ranges***	***LSB Size (Quantization Step***	***Max Sampling Rate (Single Channel***
200MHz	$\pm 10mV \sim \pm 20V$	*< 0.6% of input range*	*1GS/s*

2.3 Signal Control Module

The signal control module is used to switch the activity status between sensors and channels. PicoScope operates in single channel mode, which means that only one channel is enabled for each data acquisition as a means to enhance the resolution. In addition, the built-in PicoScope internal trigger can be used to send input signals; the internal trigger emits signals at the moment of channel switching, achieving synchronization during single channel operation.

Switching between channels was achieved with a multiplexer (MUX) built for this project, based on TMUX1109 from National Instruments. The schematic diagram is shown in Figure 3-a. DA and DB are signal inputs (D for Drain), connected to the coaxial output of the PicoScope internal trigger, where DB is the reference voltage (ground). SxA and SxB are connected to the channel x coaxial input of PicoScope, and the ultrasound sensor is parallel between SxA and SxB (S for Source), where the B end is also the reference (ground). In the operation of multiplexer, the Source terminal and Drain terminal can be exchanged, which means it could be 4 to 1 or 1 to 4 in practical use. The digital control input is from the logic signal terminal EN and the address lines A0 and A1. Table 6-2 is the truth table. In the actual process, the conductivity between Sx and D terminals is achieved by controlling the logic voltage on EN, A0, and A1, where >1.8V is considered a logic high level. The design of the circuit based on TMUX1109 is as Figure 3-b.

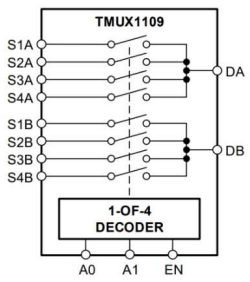

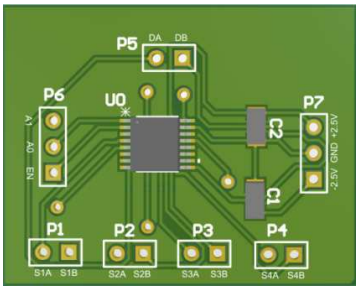

(a) (b)

Figure 3. (a) The block diagram of TMUX1109 (b)The printed circuit board design for TMUX1109

Table 2. TMUX1109 truth table (x denotes 0 or 1)

EN	***A1***	***A0***	***Connection to Drain***
0	*x*	*x*	*All OFF*
1	*0*	*0*	*S1*
1	*0*	*1*	*S2*
1	*1*	*0*	*S3*
1	*1*	*1*	*S4*

2.4 Control of the Ultrasound System

A LabVIEW virtual instrument testing platform has been developed to operate the whole system. This integrates control of the PicoScope, temperature DAQ TC08, and microcontroller Arduino Uno. The schematic diagram is shown in Figure 4. During signal acquisition, the program loads a preset signal acquisition test matrix, channel parameters, and sampling parameters. It is worth noting that in the software, the PicoScope channel opening instruction and the output port control instruction of Arduino are synchronized.

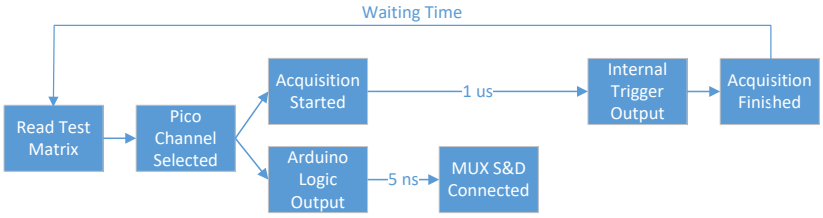

Figure 4. The diagram of ultrasound system control

For example, when the signal from A channel is to be collected, the opening of A channel is informed through the loading of the test matrix. The Arduino will send a logic high level to TMUX1109 to connect S1A to DA and S1B to DB, which means that only the sensor of A channel is connected to the signal transmission circuit and the others are separated. In addition, there is a delay of about 1μs between internal trigger initiation and PicoScope channel opening. This is much greater than the maximum transition time of TMUX1109 (usually 5ns). Therefore, each channel will be fully switched on ready for when the signals are collected.

3. Principle of Ultrasound Measurement

3.1 Ultrasound Pulse-echo Technique

The ultrasound pulse-echo method is used for measuring the real-time coating thickness; each

sensor works as both signal transmitter and receiver. When the transmitted ultrasound meets the coating-steel interface and then coating-lubricant interface, there will be two reflections. The coating thickness can be obtained by comparing the Time-of-Flight (ToF) of the two reflected signals. The expression for coating thickness d is as Equation 1, where the speed of sound c is the function of temperature T and Δt represents the ToF. The position of reflections is determined by the peak position of the reflection pulses.

$$d = c(T) \cdot \Delta t \tag{1}$$

When calculating the coating wear, two important parameters should be recorded. The first is the original thickness, which is measured before the operation. Another is the real-time temperature. The operation of the machine is a dynamic progress. Friction can change with time, resulting in a temperature change and potential coating wear. The speed of sound is a function of temperature, so it is important to record the real-time temperature to update the speed of sound. The speed of sound for the aluminium alloy has been calibrated before the in-situ operation, which is given by:

$$c_{Al}(T) = -2.26 \times T + 6477 \tag{2}$$

3.2 Simulation of the Acoustic Response of Shells with Worn Regions

A double-layer structure of an aluminium layer on a steel substrate was established for the simulation using a commercial finite element analysis software COMSOL Multiphysics. This was intended to simulate the ultrasonic response of a worn region of the thin coating on a steel backing. The parameters for the simulations are shown in Table 3.

Table 3. Properties of materials in finite element modelling

Description	***Density (g/cm^3)***	***Thickness (mm)***	***Width (mm)***	***Young's modulus (10^9 Pa)***	***Poisson's ratio***
Aluminium Coating Layer	*2.7*	*0.4*	*10*	*70*	*0.33*
Steel Bearing Layer	*7.85*	*1.1*	*10*	*205*	*0.28*
Signal Input Region	*-*	*-*	*2*	*-*	*-*

The governing equation of the elastic wave is given by Equation 3. In Equation 3, E represents the Young's modulus, ν represents Poisson's ratio and ρ is the density of the media. The displacement and boundary pressure are in vector form, $\vec{u}$ and $\vec{F}$.

$$\frac{E}{2(1+\nu)}\left[\nabla^2 \vec{u} + \frac{1}{(1-2\nu)}\nabla(\nabla \cdot \vec{u})\right] + \vec{F} = \rho \frac{\partial^2 \vec{u}}{\partial t^2} \tag{3}$$

Figure 5-a shows a cross-section image of an instrumented aluminium-alloy coated bearing shell, which has been used as the reference of modelling. The plane used to cut the bearing shell passed through the rotation axis. Figure 5-b shows an idealized flat wear scar (2mm-wide, 0.1mm-deep) under the ultrasound covered region in Figure 5-a. In Figure 5-b, the blue lines represent the ultrasound ($\vec{F}$) input area. The ultrasound transmits into the layered structure normally and its amplitude of $\vec{F}$ is given by Equation 4. PML stands for perfect matched layer,

which is used to simulate an infinite space. In Equation 4, the time step is in the range $t \epsilon [0,3/f]$, which f is the ultrasound frequency. The input region is also used as the probe to receive the reflected signals. In the simulation, the wavelength of 22MHz ultrasound in aluminium is around 286μm, and the grid size for meshing is set as 10-50μm. In the simulation, a 3-cycle Hann windowed sine wave was applied to eliminate the high-frequency responses and the energy attenuation. The zero displacement and zero velocity are set as initial conditions and all the outboard edges are set as a soft boundary where the sound pressure at the boundaries is zero.

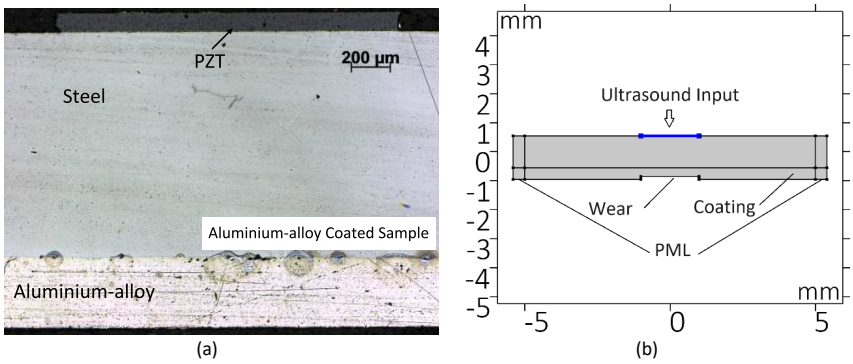

Figure 5. (a)The cross-section image of an instrumented aluminium coated bearing shell
(b)The diagram of finite element modelling, a simulation of a 2mm-wide, 0.1mm-deep wear scar

$$F = \left[1 - cos\left(\frac{2\pi f t}{3}\right)\right] \cdot sin(2\pi f t) \quad (4)$$

Based on the structure in Figure 5, a series of simulations has been performed, with the same scar width (2mm) but different scar depths, to simulate the progression of localised wear. The simulation results, displayed as the reflected waveform (A-scan) for each case, are shown in Figure 6.

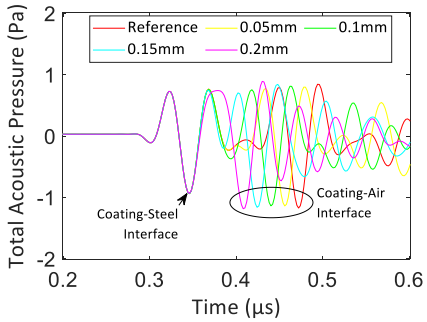

Figure 6. The simulation result of the reflection from a worn region for different wear depths

In Figure 6, the red curve represents the reference signal, which corresponds to the reflection from an undamaged surface. When the depth of wear increases, the reflection from the

Figure 8-a shows the ultrasound reflection from the two interfaces of the aluminium coating, which interface 1 represents the coating-steel interface and interface 2 represents the coating-oil interface. The blue curve is the A-scan result at the start of measurement and the red curve is collected at the end. By calculating the arrival time between the two reflections, the ultrasound ToF inside the coating can be obtained. Then, the residual coating thickness is calculated by the ToF and speed of sound, using the real-time temperature and Equation 2. Figure 8-b shows the wear progress of Sample 1 during the operation.

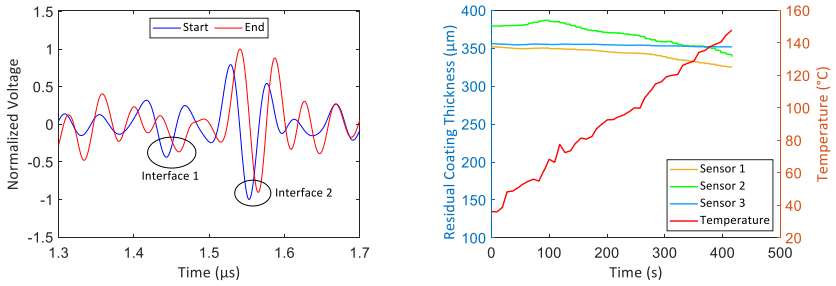

(a) (b)

Figure 8. (a) The interface reflections in ultrasound in-situ measurement
(b) Progression of wear expressed as the residual coating thickness (Sample 1)

For comparison, the wear was independently measured using a microscope Zeiss Axio Imager A2m, following the sectioning direction in Figure 7-b. The tested samples were sectioned, mounted and polished before the observation. The largest deviation occurs at Sample 1 Sensor 1, around 14µm, while most of the other sensors has a deviation less than 10µm. The sensors proved reasonably robust, with only one of 15 the sensors was failing during the test program (Sample 4, Sensor 3). The results of the five samples are shown in the charts below and summarized in Table 4. In Table 4-b, 4-c and 4-e, there are some results show that there is a negative wear value after the operation. This will be discussed in the discussion section.

Table 4. (a) The results of ultrasound in-situ wear measurement (Sample 1)

	Sensor 1	*Sensor 2*	*Sensor 3*
Thickness - Start (µm)	*351.94*	*382.54*	*356.13*
Thickness - End (µm)	*325.08*	*367.10*	*351.93*
Microscope Result (µm)	*339.19*	*369.11*	*357.15*
Deviation (µm)	*14.11*	*2.01*	*5.23*
Relative Error	*4.16%*	*0.54%*	*1.46%*
Depth of Wear (µm)	*26.87*	*15.44*	*4.21*

Table 4. (b) The results of ultrasound in-situ wear measurement (Sample 2)

	Sensor 1	*Sensor 2*	*Sensor 3*
Thickness - Start (µm)	*352.24*	*379.36*	*364.43*
Thickness - End (µm)	*354.44*	*343.10*	*358.27*
Microscope Result (µm)	*350.35*	*342.58*	*350.95*
Deviation (µm)	*4.10*	*0.53*	*7.33*
Relative Error	*1.17%*	*0.15%*	*2.09%*

Depth of Wear (µm)	*-2.20*	*36.26*	*6.15*

Table 4. (c) The results of ultrasound in-situ wear measurement (Sample 3)

	Sensor 1	*Sensor 2*	*Sensor 3*
Thickness - Start (µm)	*363.56*	*352.78*	*360.68*
Thickness - End (µm)	*365.23*	*336.02*	*360.90*
Microscope Result (µm)	*361.77*	*341.61*	*352.32*
Deviation (µm)	*3.46*	*5.60*	*8.58*
Relative Error	*0.96%*	*1.64%*	*2.44%*
Depth of Wear (µm)	*-1.67*	*16.77*	*-0.22*

Table 4. (d) The results of ultrasound in-situ wear measurement (Sample 4)

	Sensor 1	*Sensor 2*	*Sensor 3*
Thickness - Start (µm)	*365.85*	*375.01*	*-*
Thickness - End (µm)	*356.91*	*368.04*	*-*
Microscope Result (µm)	*346.55*	*360.31*	*-*
Deviation (µm)	*10.36*	*7.73*	*-*
Relative Error	*2.99%*	*2.15%*	*-*
Depth of Wear (µm)	*8.94*	*6.97*	*-*

Table 4. (e) The results of ultrasound in-situ wear measurement (Sample 5)

	Sensor 1	*Sensor 2*	*Sensor 3*
Thickness - Start (µm)	*345.99*	*370.35*	*357.11*
Thickness - End (µm)	*348.58*	*361.64*	*356.05*
Microscope Result (µm)	*349.04*	*351.85*	*349.21*
Deviation (µm)	*0.46*	*9.79*	*6.84*
Relative Error	*0.13%*	*2.78%*	*1.96%*
Depth of Wear (µm)	*-2.59*	*8.71*	*1.07*

Figure 9 shows the wear progression for the rest of four samples during the test. Concerning the temperature change, started from Sample 3, the ultrasound data was continually collected during cooling-down. During that period, the apparent measured thickness rises slightly, this demonstrates the imperfect temperature compensation of the speed of sound and the resulting effect on the wear measurement. But according to the thickness variation shown in Figures 9-b, 9-c and 9-d, generally temperature changes is well compensated and the final ultrasound results are similar to the microscope results.

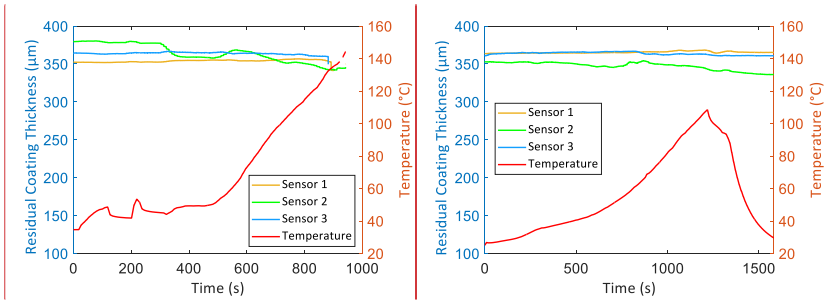

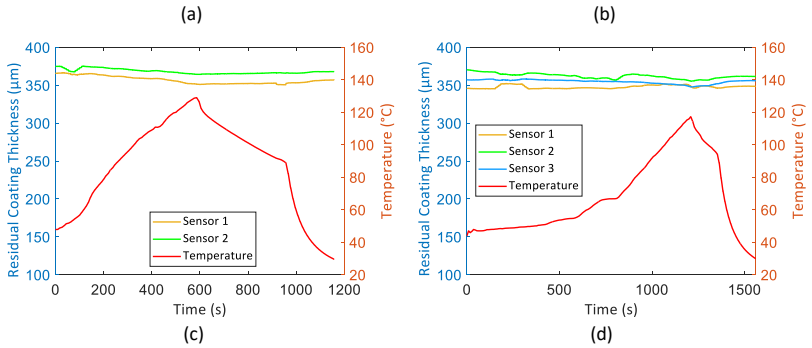

Figure 9. Progression of wear expressed as the residual coating thickness
(a)Sample 2 (b)Sample 3 (c)Sample 4 (d)Sample 5

Based on the calculated values of wear depth in Table 4, the wear process of the aluminium alloy coated samples can be divided into two cases. The wear rates of Sample 1 and Sample 4 are similar, where the wear at Sensor 1 is greater than that at Sensor 2, while Sensor 3 is not considered as Sample 4 Sensor 3 has already failed. Samples 2, 3, and 5 have the highest wear reading at Sensor 2 (middle), while the wear at Sensors 1 and 3 (at the sides) is similar and almost undamaged. Moreover, there is a common characteristic of the five samples that the wear at Sensor 3 is relatively low. It is speculated that during testing, the thermocouple was fixed between Sensor 1 and Sensor 2, resulting in uneven local load distribution.

4.3 An On-line Measurement under Oil Starvation

The repeatability of the results in Section 4.2 demonstrates that the in-situ ultrasound measurement functions satisfactorily under mixed lubrication. In this section, operation under oil starvation (i.e. boundary regime) is explored. It is worth noting that a small quantity of engine oil was added during the operation, when an excessive torque was detected to avoid seizure. Figure 10 shows several temperature changes at around 500s, which were caused by the addition of fresh lubricant.

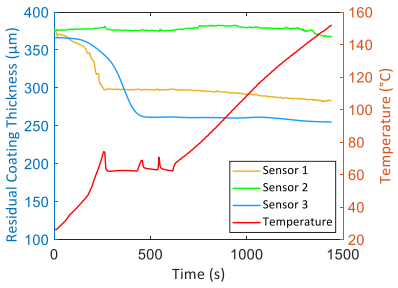

Figure 10. The curve of bearing wear process of on-line ultrasound measurement (oil starvation)

In Figure 10, the coating under Sensor 2 shows a slight wear which is different with the wear

results in section 4.2. This is because the lubricant was initially fed near the Sensor 2 area, which protected this area from the start. However, the wear rate at Sensor 1 and 3 was high initially, then decreased after the first and second lubricant additions, indicating that lubricant was protecting the bearing surface from further damage. The comparison between the ultrasound and microscope results is shown in Table 5. The deviation was around 6µm and can be regarded reliable.

Table 5. The results of ultrasound in-situ wear measurement (oil starvation)

	Sensor 1	*Sensor 2*	*Sensor 3*
Thickness - Start (µm)	*371.39*	*376.26*	*366.25*
Thickness - End (µm)	*282.92*	*368.12*	*254.87*
Microscope Result (µm)	*282.69*	*361.71*	*248.23*
Deviation (µm)	*0.23*	*6.41*	*6.64*
Error	*0.08%*	*1.77%*	*2.67%*
Depth of Wear (µm)	*88.46*	*8.14*	*111.38*

5. Discussion

5.1 The Failure of Ultrasound Sensor during Measurement

One of the sensors failed during testing. The electrical contacts of Sample 4 Sensor 3 were checked after the operation and showed to be peeling away from the sensor. A possible reason for this failure is illustrated in Figure 11.

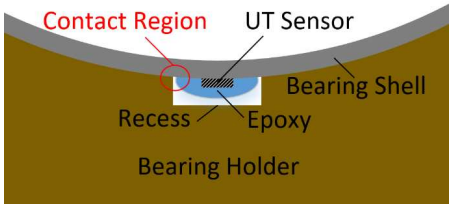

Figure 11. The diagram of the contact between epoxy protection and bearing holder

Figure 11 shows the contact between the epoxy protection and the bearing holder. The bearing shell was clamped onto the bearing holder and the sensors and protection should be located freely within the recess. However, during the bearing installation, there may have been a contact between the recess and the epoxy protection, as the red circle in Figure 11, which could lead to a shear stress to the epoxy protection and peel the sensor off from the bearing. Therefore, during the instrumentation, the sensors need to be mounted precisely onto the bearing shell with enough space such that no contact occurs with the housing.

5.2 The Negative Value of Some Wear Results

In Table 4, it is worth noting that there are four sensors (Sample 2 Sensor 1, Sample 3 Sensor

1, Sample 3 Sensor 3, Sample 5 Sensor 1) showing a small negative wear value, corresponding to a coating thickness increase. One possible explanation is that the temperature of the bearing and coating changes over time, and the previous results of the speed of sound calibration of the coating material are not fully accurate. This may have some small deviations, or the detection value from thermocouples may also have small test errors.

Another possible reason is that the worn surface is not smooth, as the example of the area under Sample 5 Sensor 1 in Figure 12-a.

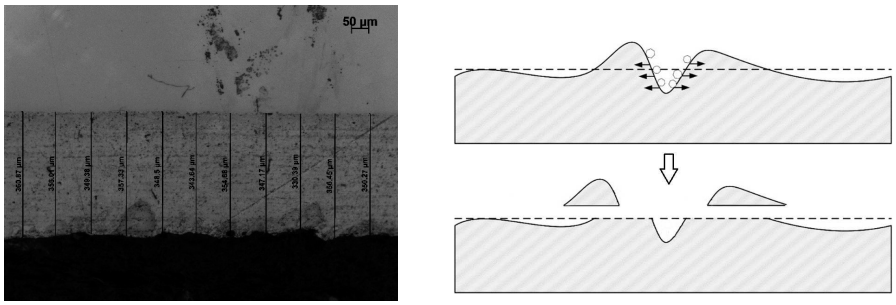

(a) (b)

Figure 12. (a) The cross-section view of the damaged surface (Sample 5, Sensor 1)
(b) The initial stage of a surface wear and the diagram of wear process

The ultrasound measured a flat surface before testing and a rough surface afterwards. At the early stage of a wear, the material near the surface is pressed and scratched by some hard particles or the asperities on the shaft. A new surface profile is formed subsequently, which is locally shown as a thinner wall in the middle and a thicker wall at both sides, as Figure 12-b. The coating materials are extruded laterally and the material above the dashed line will be removed after a short-time operation. During the ultrasound measurement this type of damage will appear as a similar thickness, or even thicker, compared with an undamaged surface. For example, in Figure 8-b, the wear process of Sample 1 Sensor 2, it shows a thickness increase at around 100s and in Figure 9-a, the wear process of Sample 2 Sensor 2, it also shows an increase at around 600s. In this case, when there is an increase of thickness derived by ultrasound signal, it can be estimated that the surface is starting to become damaged.

6. Conclusion

An ultrasound in-situ measurement system for detecting wear in plain bearing shells is proposed. The ultrasound instrumentation is based around shell-mounted 22MHz sensors, a DAQ module made up of an ultrasonic multiplexer (TMUX1109), a digital oscilloscope, and an Arduino micro-controller. The approach has been shown to measure the real-time thickness of an aluminium bearing coating less than 370µm during operation.

A numerical simulation was used to show the relationship between ultrasound and thickness

reduction. A 22MHz ultrasound input was virtually used to measure 50µm-200µm surface wears on a 400µm aluminium coating. It shows that when the depth of wear increases, the reflection from the coating-air interface moves closer towards that from the coating-steel interface.

A series of in-situ experiments was performed on a bearing shell in a rotary tribometer. Five samples were tested in the mixed lubrication condition and the wear progression has been plotted. The deviation between the ultrasound and an independent microscope measurement at the end state are generally less than 10µm (<3%), with a maximum deviation of 14.11µm (4.16%). An extra oil starvation test has been carried out and it shows a severe wear process and the difference between ultrasound and microscope result was around 6µm (<2.67%).

In general, the in-situ ultrasound wear measurement system can achieve an accurate monitoring of the coating condition of a bearing in operation and as precise as that measured using a microscope. The design of the system enables the sensors to be easily installed and bearings are easily replaced. The small size sensors are suitable for use in inaccessible conditions, such as the wind turbine and stern tube bearings, to achieve a real-time monitoring and reduce the cost of maintenance.

7. Reference

[1] K. Ono, S. Murashita, and H. Yamaura, “Stability analysis of a disk-spindle supported by a plain journal bearing and pivot bearing,” *Microsystem Technologies*, vol. 11, no. 8–10, pp. 734–740, Aug. 2005, doi: 10.1007/s00542-005-0574-9.

[2] F. A. Davis and T. S. Eyre, “Wear of plain bearing materials with particular reference to role of soft phases,” *Materials Science and Technology*, vol. 7, no. 8, pp. 746–756, Aug. 1991, doi: 10.1179/mst.1991.7.8.746.

[3] M. S. Ali, P. A. S. Reed, S. Syngellakis, A. J. Moffat, and C. Perrin, “Microstructural Factors Affecting Fatigue Initiation in Various Al Based Bearing Alloys,” *Materials Science Forum*, vol. 519–521, no. PART 2, pp. 1071–1076, Jul. 2006, doi: 10.4028/www.scientific.net/MSF.519-521.1071.

[4] S. B. Palmer, S. Dixon, B. Lanyon, and G. Rowlands, “Measurement of coating thickness using ultrasonic resonance spectroscopy,” in *Advanced Sensor Technologies for Nondestructive Evaluation and Structural Health Monitoring II*, SPIE, Mar. 2006, p. 61790B. doi: 10.1117/12.654753.

[5] J. Kanja, R. Mills, X. Li, H. Brunskill, A. K. Hunter, and R. S. Dwyer-Joyce, “Non-contact measurement of the thickness of a surface film using a superimposed ultrasonic standing wave,” *Ultrasonics*, vol. 110, Feb. 2021, doi: 10.1016/j.ultras.2020.106291.

[6] M. Long and H. J. Rack, “Ultrasonic in situ continuous wear measurements of orthopaedic titanium alloys,” *Wear*, vol. 205, no. 1–2, pp. 130–136, Apr. 1997, doi: 10.1016/S0043-1648(96)07233-X.

[7] H. Brunskill, P. Harper, and R. Lewis, “The real-time measurement of wear using ultrasonic reflectometry,” *Wear*, vol. 332–333, pp. 1129–1133, May 2015, doi: 10.1016/j.wear.2015.02.049.

[8] F. Honarvar, F. Salehi, V. Safavi, A. Mokhtari, and A. N. Sinclair, “Ultrasonic monitoring

of erosion/corrosion thinning rates in industrial piping systems," in *Ultrasonics*, Sep. 2013, pp. 1251–1258. doi: 10.1016/j.ultras.2013.03.007.